Eur. Phys. J. C (2024) 84:841
https://doi.org/10.1140/epjc/s10052-024-13210-w

THE EUROPEAN PHYSICAL JOURNAL C



Regular Article - Theoretical Physics

# Distinguishing signature of Kerr-MOG black hole and superspinar via Lense–Thirring precession

**Parthapratim Pradhan**[a]

Department of Physics, Hiralal Mazumdar Memorial College for Women, Dakshineswar, Kolkata 700035, India

Received: 17 June 2024 / Accepted: 4 August 2024


**Abstract** We examine the geometrical differences between the black hole (BH) and naked singularity (NS) or superspinar via Lense–Thirring (LT) precession in spinning modified-gravity (MOG). For *BH* case, we show that the LT precession frequency ($\Omega_{LT}$) along the pole is proportional to the angular-momentum ($J$) parameter or spin parameter ($a$) and is inversely proportional to the cubic value of radial distance parameter, and also governed by Eq. (1). Along the equatorial plane it is governed by Eq. (2). While for *superspinar*, we show that the LT precession frequency is inversely proportional to the cubic value of the spin parameter and it decreases with distance by MOG parameter as derived in Eq. (3) at the pole and in the limit $a >> r$ (where $a$ is spin parameter). For $\theta \neq \frac{\pi}{2}$ and in the superspinar limit, the spin frequency varies as $\Omega_{LT} \propto \frac{1}{a^3 \cos^4\theta}$ and by Eq. (38).

## 1 Introduction

The fundamental difference between a black hole (BH) and a naked singularity (NS)[1] is that the former has a horizon structure while the latter doesn't have any horizon structure. Once more a BH is of two types: non-extremal black hole (NXBH) and extremal black hole (XBH). A NXBH is identified by non-zero surface gravity ($\kappa \neq 0$) while XBH is identified by *zero* surface gravity ($\kappa = 0$). For NS the surface gravity is undefined because it has no horizon. So, how one can differentiate between these three compact objects? This is an intriguing topic of research both in astrophysics and in general relativity. Therefore, in this Letter we want to find out that the distinction between these three compact objects by using LT precession frequency [1–4].

For spinning Kerr BH in general relativity, the LT precession frequency varies as spin parameter and is inversely proportional to the cubic value of radial distance both along the polar axis and the equatorial plane. While for Kerr NS or superspinar, the LT frequency varies as radial distance and inversely proportional to the cubic value of the spin parameter along the pole. This is the fundamental difference between BH and superspinar in the general relativity. Now we will examine what happens this situation in case of other alternative gravity theory i.e. Kerr-MOG gravity?

Consequently we have considered a spinning compact object such as Kerr-MOG BH in MOG theory [9–11]. It is described by mass parameter ($\mathcal{M}$), spin parameter ($a$) and a deformation parameter or MOG parameter ($\alpha$). In contrast to Kerr BH, which is described only by the mass parameter and the spin parameter. The MOG theory was proposed by Moffat [10]. It was sometimes reffered to as scalar-tensor-vector gravity (STVG) theory. The main concept in MOG theory is that the BH charge parameter is proportional to the mass parameter i. e. $Q = \sqrt{\alpha G_N} M$ [9]. Where $\alpha = \frac{G-G_N}{G_N}$ should be measured deviation of MOG from GR. The MOG theory proves several interesting features like superradiance [13], the quasinormal modes and the ring down of BH mergers [12]. Apart from that MOG theory obeys an action principle formulation, and the weak equivalence principle. The details of MOG theory and action formulation could be found in the following works [9,11–13]. So, we have not discussed it in detail here.

The metric for static spherically-symmetric BH in MOG theory can be obtained by substituting $\mathcal{Q} = \sqrt{\alpha G_N} M$ in the usual Reissner–Nordström BH solution. Similarly, one can derive the Kerr-MOG BH by putting this condition in Kerr–Newman BH.

In [5], we have derived in detail the generalized spin precession frequency of a test gyroscope around the Kerr-MOG BH. Using this frequency expression, we differentiated the

[1] When no event horizons are formed during gravitational collapse then it is called as NS or superspinar [29]. It is unstable compact object.

[a] e-mail: ppradhan77@gmail.com (corresponding author)

Published online: 21 August 2024

behavior of three compact objects i.e. NXBH, XBH, and NS. Here, we focus on particularly LT frequency by taking the limit i.e. angular velocity $\Omega = 0$ in generalized spin frequency expression.

For Kerr BH [6] (see also [7,8]), it was demonstrated that a clear distinction between these compact objects. In fact they have found that the LT frequency varies as $\Omega_{LT} \propto a$ and $\Omega_{LT} \propto \frac{1}{r^3}$. While for Kerr-NS (or superspinar) and also in the limit $a >> r$[2] and in the region $\theta \neq \frac{\pi}{2}$ the LT frequency varies as $\Omega_{LT} \propto r$ and $\Omega_{LT} \propto \frac{1}{a^3}$. In the present work, we would like to examine this scenario in the MOG theory specifically for Kerr-MOG BH.

In the present work, we derive the following results:

(i) We show that for *NXBH* the LT precession frequency along the pole is directly proportional to the spin parameter ($a$), and is inversely proportional to the cubic value of radial distance parameter, and

$$\Omega_{LT} \propto \left[1 - \left(\frac{\alpha}{1+\alpha}\right)\frac{G_N\mathcal{M}}{2r}\right] \times \left(1 - 2\frac{G_N\mathcal{M}}{r} + \frac{a^2 + \left(\frac{\alpha}{1+\alpha}\right)G_N^2\mathcal{M}^2}{r^2}\right)^{-1} \quad (1)$$

(ii) Along the equatorial plane, the LT precession frequency is directly proportional to the spin parameter, and is inversely proportional to the cubic value of radial distance, and

$$\Omega_{LT} \propto \left[1 - \left(\frac{\alpha}{1+\alpha}\right)\frac{G_N\mathcal{M}}{r}\right] \times \left(1 - 2\frac{G_N\mathcal{M}}{r} + \frac{\left(\frac{\alpha}{1+\alpha}\right)G_N^2\mathcal{M}^2}{r^2}\right)^{-1} \quad (2)$$

(iii) For *XBH*, we determine the LT frequency is proportional to the angular-momentum ($J$) parameter i.e. $\Omega_{LT} \propto \frac{\mathcal{M}^2}{\sqrt{1+\alpha}}$ and is inversely proportional to the cubic value of radial parameter i.e. $\Omega_{LT} \propto \frac{1}{r^3}$.

(iv) While for *superspinar*, the $\Omega_{LT}$ along the pole and in the region $a >> r$ should be

$$\Omega_{LT} \propto \left[r - \left(\frac{\alpha}{1+\alpha}\right)\frac{G_N\mathcal{M}}{2}\right]\left[1 + \left(\frac{\alpha}{1+\alpha}\right)\frac{G_N^2\mathcal{M}^2}{a^2}\right]^{-\frac{1}{2}} \quad (3)$$

(v) For $\theta \neq \frac{\pi}{2}$ and in the superspinar limit, we find

$$\Omega_{LT} \propto \frac{1}{a^3\cos^4\theta} \quad (4)$$

and Eq. (38). Interestingly, the LT precession frequency is inversely proportional to the both $a^3$ and $\cos^4\theta$ factor in the superspinar limit.

There are several discussions regarding the Kerr NS such as stability issue, thermodynamic properties, effect of gravitational self-force (GSF), effect of conservative self-force and the implications of Polish doughnut model etc. They could be found in the following Refs. [19–27]. So, the NS is an interesting topic of research in recent times both from the theoretical and observational point of view.

In the next section, we will study the spin precession frequency in Kerr BH in MOG theory and show that the structural variation of three compact objects: NXBH, XBH and NS. In Sect. 3, we have given the conclusions.

## 2 Spin precession frequency in Kerr-MOG BH

To distinguish NXBH, XBH and NS in Kerr-MOG BH, we have to write the LT spin precession expression in terms of Boyer–Lindquist coordinates [5] (see also [14–18]) as

$$\boldsymbol{\Omega}_{LT} = \frac{-\sqrt{g_{rr}}\,\mathcal{A}\hat{r} + \sqrt{g_{\theta\theta}}\,\mathcal{F}\hat{\theta}}{2\sqrt{-g}\,g_{tt}} \quad (5)$$

where

$$\mathcal{A} = g_{tt}\,g_{t\phi,\theta} - g_{t\phi}\,g_{tt,\theta} \quad (6)$$

$$\mathcal{F} = g_{tt}\,g_{t\phi,r} - g_{t\phi}\,g_{tt,r} \quad (7)$$

and $g$ is the determinant of the metric tensor. This is the exact LT precession frequency of a test gyro due to rotation of any stationary and axisymmetric spacetime.

The most interesting feature of Eq. (5) is that it should be applicable for any stationary axisymmetric BH spacetime which is valid for both outside and inside the ergosphere. Here, we are particularly interested in the limit $\Omega = 0$. The case of $\Omega \neq 0$ is discussed and analyzed in the work [5].

Our next task is to write the metric explicitly for KMOG BH as described in Ref. [9]

$$ds^2 = -\frac{\Delta}{\rho^2}\left[dt - a\sin^2\theta d\phi\right]^2 + \frac{\sin^2\theta}{\rho^2}\left[(r^2+a^2)\,d\phi - a dt\right]^2 + \rho^2\left[\frac{dr^2}{\Delta} + d\theta^2\right]. \quad (8)$$

where

$$\rho^2 \equiv r^2 + a^2\cos^2\theta$$

[2] The region $a >> r$ is a typical nature of Kerr naked singularities [7].

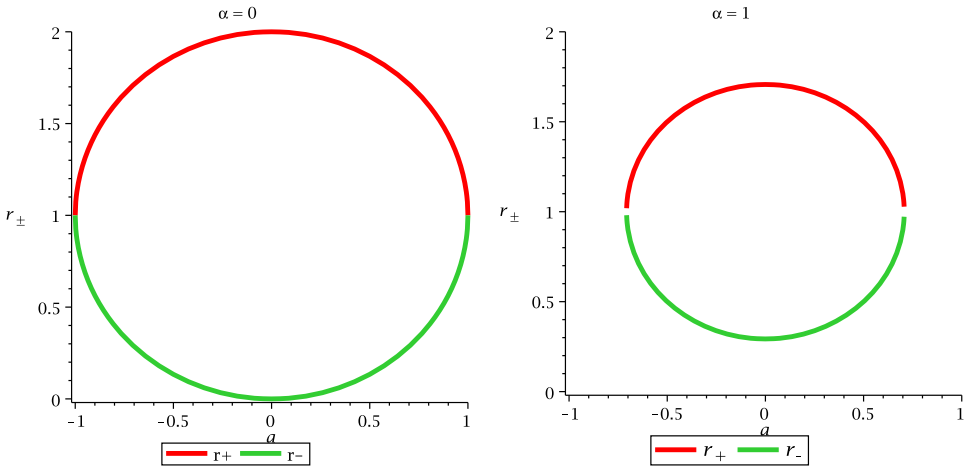


**Fig. 1** The figure describes the variation of $r_{\pm}$ with $a$ for Kerr BH and Kerr-MOG BH. Left figure for Kerr BH. Right figure for Kerr-MOG BH. The presence of the MOG parameter is deformed the shape of the horizon radii

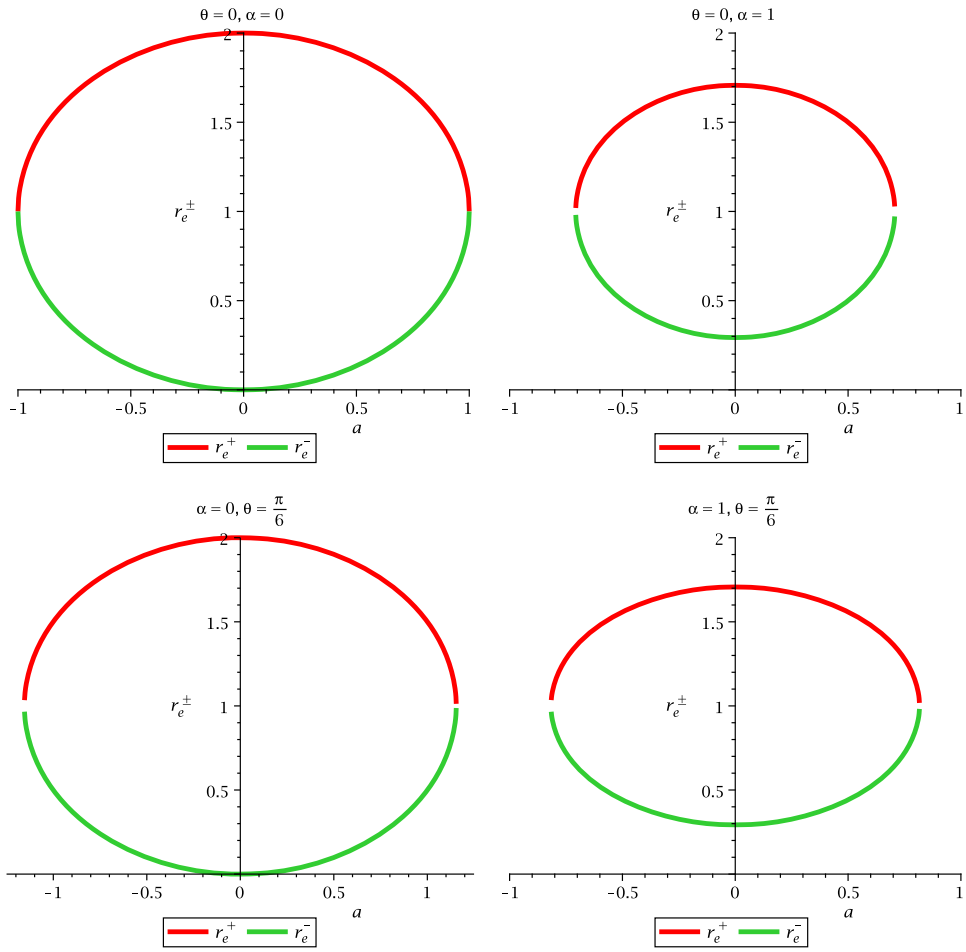


**Fig. 2** The figure indicates the variation of $r_e^{\pm}(\theta)$ with $a$ for Kerr BH and Kerr-MOG BH

$$\Delta \equiv r^2 - 2G_N(1+\alpha)Mr + a^2 + G_N^2\alpha(1+\alpha)M^2. \quad (9)$$

where $G_N$ is Newton's gravitational constant and $M$ is BH mass. We should mention that in the metric $c = 1$.[3] The above metric is an axially-symmetric and stationary spacetime. The ADM mass and angular momentum are computed in [28] as $\mathcal{M} = (1+\alpha)M$ and $J = aG_N\mathcal{M}$.[4] We consider here the ADM mass throughout the paper for our convenience. Substituting these values in Eq. (9) then $\Delta$ becomes

$$\Delta = r^2 - 2G_N\mathcal{M}r + a^2 + \frac{\alpha}{1+\alpha}G_N^2\mathcal{M}^2 \quad (10)$$

[3] We have used the geometrical units i. e. $c = 1$. The signature of the metric becomes $(-,+,+,+)$.

[4] One could determine the relation between the BH mass and ADM mass as $M = \frac{\mathcal{M}}{1+\alpha}$.

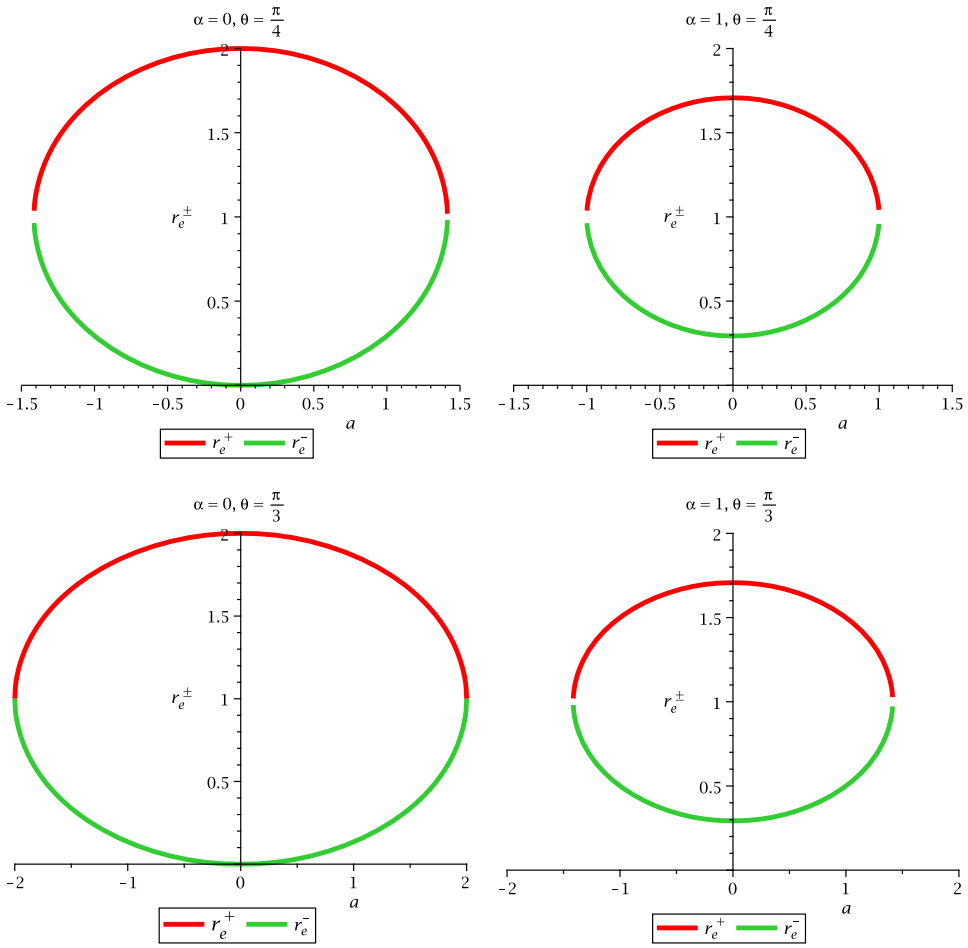


**Fig. 3** The figure indicates the variation of $r_e^{\pm}(\theta)$ with $a$ for Kerr BH and Kerr-MOG BH

The above metric describes a BH with double horizon

$$r_+ = G_N\mathcal{M} + \sqrt{\frac{G_N^2\mathcal{M}^2}{1+\alpha} - a^2},$$
$$r_- = G_N\mathcal{M} - \sqrt{\frac{G_N^2\mathcal{M}^2}{1+\alpha} - a^2}. \tag{11}$$

where $r_+$ is called as event horizon and $r_-$ is called as Cauchy horizon.

Note that $r_+ > r_-$. Differences between the horizon structure in the presence of MOG parameter and without MOG parameter could be seen visually in the Fig. 1.

It should be noted that when $\alpha = 0$, one gets the horizon radii of Kerr BH. The NXBH, XBH and NS solutions do exist in the following range

$$\frac{a^2}{G_N^2\mathcal{M}^2} < \frac{1}{1+\alpha} \quad \text{NXBH} \tag{12}$$
$$\frac{a^2}{G_N^2\mathcal{M}^2} = \frac{1}{1+\alpha} \quad \text{XBH} \tag{13}$$
$$\frac{a^2}{G_N^2\mathcal{M}^2} > \frac{1}{1+\alpha} \quad \text{NS} \tag{14}$$

Note that the MOG parameter or deformation parameter ($\alpha$) is always positive definite. If we invert the above inequality then one gets the restriction on $\alpha$. We have tabulated the values of spin parameter for various values of MOG parameter.

| $\alpha$ | NXBH | XBH | NS |
|---|---|---|---|
| $\alpha = 0$ | $a = 0.5$ | $a = 1$ | $a = 2$ |
| $\alpha = 1$ | $a = 0.4$ | $a = \frac{1}{\sqrt{2}} = 0.7$ | $a = 0.9$ |
| $\alpha = 2$ | $a = 0.3$ | $a = \frac{1}{\sqrt{3}} = 0.57$ | $a = 0.7$ |
| $\alpha = 3$ | $a = 0.2$ | $a = \frac{1}{2} = 0.5$ | $a = 0.8$ |
| $\alpha = 4$ | $a = 0.2$ | $a = \frac{1}{\sqrt{5}} = 0.44$ | $a = 0.6$ |
| $\alpha = 5$ | $a = 0.2$ | $a = \frac{1}{\sqrt{6}} = 0.4$ | $a = 0.5$ |
| $\alpha = 6$ | $a = 0.2$ | $a = \frac{1}{\sqrt{7}} = 0.37$ | $a = 0.4$ |
| $\alpha = 8$ | $a = 0.2$ | $a = \frac{1}{3} = 0.33$ | $a = 0.5$ |
| $\alpha = 10$ | $a = 0.2$ | $a = \frac{1}{\sqrt{11}} = 0.3$ | $a = 0.5$ |

The outer ergosphere is situated at

$$r = r_e^+(\theta) = G_N\mathcal{M} + \sqrt{\frac{G_N^2\mathcal{M}^2}{1+\alpha} - a^2\cos^2\theta}. \tag{15}$$

and the inner ergosphere is situated at

$$r = r_e^-(\theta) = G_N\mathcal{M} - \sqrt{\frac{G_N^2\mathcal{M}^2}{1+\alpha} - a^2\cos^2\theta}. \tag{16}$$

and they should satisfy the following inequality $r_e^-(\theta) \leq r_- \leq r_+ \leq r_e^+(\theta)$. It may be noted that $r_e^+$ and $r_e^-$ coincide with $r_+$ and $r_-$ at the pole. The radii of ergo-region becomes imaginary for all values of $\theta$: i.e. $\theta > \cos^{-1}\left[\frac{1}{\sqrt{1+\alpha}}\left(\frac{1}{a_*}\right)\right]$. In the range $\theta < \cos^{-1}\left[\frac{1}{\sqrt{1+\alpha}}\left(\frac{1}{a_*}\right)\right]$ the radii of ergo-region becomes real and where $a_* = \frac{a}{G_N\mathcal{M}}$.

The structural differences of the outer and inner ergosphere in the presence of MOG parameter and without MOG parameter could be seen from Figs. 2 and 3. From these figures one can easily observed that the size of the ergo-sphere increases when one goes to the equator starting from pole. It becomes maximum at the equator.

In the extremal limit, the outer horizon and inner horizon coincide at $r_+ = r_- = G_N\mathcal{M}$. Thus the outer and inner ergosphere radius reduces to

$$r_e^+(\theta) = G_N\mathcal{M}\left(1 + \frac{\sin\theta}{\sqrt{1+\alpha}}\right),$$

$$r_e^-(\theta) = G_N\mathcal{M}\left(1 - \frac{\sin\theta}{\sqrt{1+\alpha}}\right). \tag{17}$$

On axis and on equatorial plane, these values are

$$r_e^{\pm}(\theta)|_{\theta=0} = G_N\mathcal{M} = r_{\pm}, \quad \text{(on axis)} \tag{18}$$

$$r_e^{\pm}(\theta)|_{\theta=\frac{\pi}{2}} = G_N\mathcal{M}\left(1 \pm \frac{1}{\sqrt{1+\alpha}}\right) = r_{\pm}|_{a=0} \quad \text{(equatorial plane)}. \tag{19}$$

In the limit $\alpha = 0$,

$$r_e^+(\theta)|_{\theta=\frac{\pi}{2}} = 2G_N\mathcal{M}, \quad r_e^-(\theta)|_{\theta=\frac{\pi}{2}} = 0. \tag{20}$$

This surface is outer to the event horizon or outer horizon and it coincides with the outer horizon at the poles $\theta = 0$ and $\theta = \pi$.

Now using the formula (5), one obtains the LT frequency vector for the metric (8)

$$\boldsymbol{\Omega}_{LT} = \frac{\chi(r)\sqrt{\Delta}\cos\theta\,\hat{r} + \mu(r)\,\sin\theta\,\hat{\theta}}{\sigma(r)}, \tag{21}$$

where

$$\chi(r) = a\Pi_\alpha$$
$$\Pi_\alpha = 2G_N\mathcal{M}r - \frac{\alpha}{1+\alpha}G_N^2\mathcal{M}^2$$
$$\mu(r) = aG_N\mathcal{M}(r^2 - a^2\cos^2\theta) - \frac{\alpha}{1+\alpha}G_N^2\mathcal{M}^2ar$$
$$\sigma(r) = \rho^3(\rho^2 - \Pi_\alpha)$$

The magnitude of this vector is computed to be

$$\Omega_{LT}(r,\theta) = \frac{\sqrt{\Delta\,\chi^2(r)\,\cos^2\theta + \mu^2(r)\,\sin^2\theta}}{\sigma(r)} \tag{22}$$

After substituting the values of $\Delta$, $\mu(r)$, $\chi(r)$, $\sigma(r)$ and $\rho$, we get the LT precession frequency for *NXBH* is

$$\Omega_{LT} = \frac{J}{r^3}\,\Upsilon(r,a,\theta,\alpha) \tag{23}$$

where

$$\Upsilon(r,a,\theta,\alpha) \equiv \Upsilon$$

and

$$\Upsilon = \frac{\sqrt{4\left[1 - \left(\frac{\alpha}{1+\alpha}\right)\frac{G_N\mathcal{M}}{2r}\right]^2\left[1 - 2\frac{G_N\mathcal{M}}{r} + \frac{a^2+\left(\frac{\alpha}{1+\alpha}\right)G_N^2\mathcal{M}^2}{r^2}\right]\cos^2\theta + \sin^2\theta\left[1 - \frac{a^2\cos^2\theta}{r^2} - \left(\frac{\alpha}{1+\alpha}\right)\frac{G_N\mathcal{M}}{r}\right]^2}}{\left(1 + \frac{a^2\cos^2\theta}{r^2}\right)^{\frac{3}{2}}\left(1 - 2\frac{G_N\mathcal{M}}{r} + \frac{a^2\cos^2\theta + \left(\frac{\alpha}{1+\alpha}\right)G_N^2\mathcal{M}^2}{r^2}\right)} \tag{24}$$

Now we will compute the precession frequency along the pole and equatorial plane for NXBH separately.

Case I: At the pole ($\theta = 0$), the LT precession frequency is

$$\Omega_{LT} = \frac{2J}{r^3}\left[1 - \left(\frac{\alpha}{1+\alpha}\right)\frac{G_N\mathcal{M}}{2r}\right]\left(1 + \frac{a^2}{r^2}\right)^{-\frac{3}{2}} \times \left(1 - 2\frac{G_N\mathcal{M}}{r} + \frac{a^2 + \left(\frac{\alpha}{1+\alpha}\right)G_N^2\mathcal{M}^2}{r^2}\right)^{-1} \tag{25}$$

It indicates that the LT precession frequency along the pole is directly proportional to the angular-momentum parameter, and is inversely proportional to the cubic value of radial distance and

$$\Omega_{LT} \propto \left[1 - \left(\frac{\alpha}{1+\alpha}\right)\frac{G_N\mathcal{M}}{2r}\right] \times \left(1 - 2\frac{G_N\mathcal{M}}{r} + \frac{a^2 + \left(\frac{\alpha}{1+\alpha}\right)G_N^2\mathcal{M}^2}{r^2}\right)^{-1} \tag{26}$$

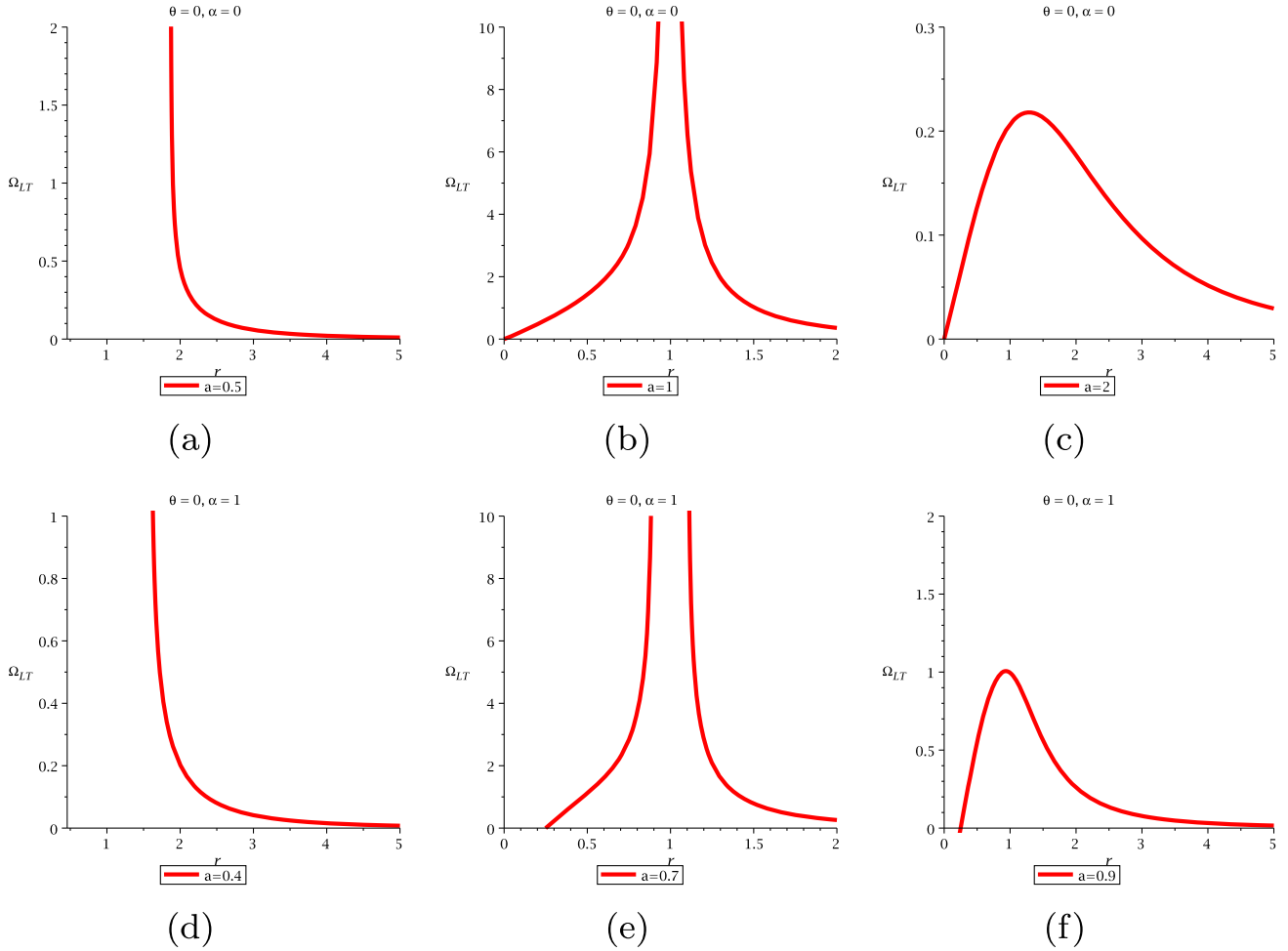


**Fig. 4** The structural variation of $\Omega_{LT}$ versus $r$ for $\theta = 0$ in KMOG with variation of MOG parameter and spin parameter. The first figure describes the variation of $\Omega_{LT}$ with $r$ for NXBH, XBH and NS without MOG parameter. The rest of the figure describes the variation of $\Omega_{LT}$ with $r$ for NXBH, XBH and NS with MOG parameter. Using these plots one can easily distinguish these three compact objects

Case II: At the equatorial plane ($\theta = \frac{\pi}{2}$), the LT precession frequency is

$$\Omega_{LT} = \frac{J}{r^3}\left[1 - \left(\frac{\alpha}{1+\alpha}\right)\frac{G_N\mathcal{M}}{r}\right] \times \left(1 - 2\frac{G_N\mathcal{M}}{r} + \frac{\left(\frac{\alpha}{1+\alpha}\right)G_N^2\mathcal{M}^2}{r^2}\right)^{-1} \tag{27}$$

Analogously, at the equatorial plane the LT precession frequency is directly proportional to the angular-momentum parameter, and is inversely proportional to the cubic value of radial distance and

$$\Omega_{LT} \propto \left[1 - \left(\frac{\alpha}{1+\alpha}\right)\frac{G_N\mathcal{M}}{r}\right] \times \left(1 - 2\frac{G_N\mathcal{M}}{r} + \frac{\left(\frac{\alpha}{1+\alpha}\right)G_N^2\mathcal{M}^2}{r^2}\right)^{-1} \tag{28}$$

For *XBH*, the LT frequency is derived to be

$$\Omega_{LT} = \frac{\Upsilon(r,\theta,\alpha)}{r^3}\frac{G_N^2\mathcal{M}^2}{\sqrt{1+\alpha}} \tag{29}$$

where

$$\Upsilon(r,\theta,\alpha)=\frac{\sqrt{4\left[1-\left(\frac{\alpha}{1+\alpha}\right)\frac{G_N\mathcal{M}}{2r}\right]^2\left(1-\frac{G_N\mathcal{M}}{r}\right)^2\cos^2\theta+\sin^2\theta\left[1-\frac{G_N^2\mathcal{M}^2}{1+\alpha}\frac{\cos^2\theta}{r^2}-\left(\frac{\alpha}{1+\alpha}\right)\frac{G_N\mathcal{M}}{r}\right]^2}}{\left(1+\frac{G_N^2\mathcal{M}^2}{1+\alpha}\frac{\cos^2\theta}{r^2}\right)^{\frac{3}{2}}\left[1-2\frac{G_N\mathcal{M}}{r}+\frac{G_N^2\mathcal{M}^2}{r^2}\left(\frac{\cos^2\theta+\alpha}{1+\alpha}\right)\right]} \tag{30}$$

Finally for *NS* and in the regime $a >> r$, the LT frequency is computed to be

$$\Omega_{LT}=\frac{\sqrt{\left[a^2+\left(\frac{\alpha}{1+\alpha}\right)G_N^2\mathcal{M}^2\right]\left[2G_N\mathcal{M}r-\left(\frac{\alpha}{1+\alpha}\right)G_N^2\mathcal{M}^2\right]^2\cos^2\theta+\left[G_N\,\mathcal{M}\,a^2\cos^2\theta+\left(\frac{\alpha}{1+\alpha}\right)G_N^2\mathcal{M}^2\,r\right]^2\sin^2\theta}}{a^2\cos^3\theta\left[a^2\cos^2\theta+\left(\frac{\alpha}{1+\alpha}\right)G_N^2\,\mathcal{M}^2\right]} \tag{33}$$

Similarly, we compute the precession frequency along the pole and equatorial plane separately.

Case I: Along the pole ($\theta = 0$), the LT precession frequency is

$$\Omega_{LT}=\frac{G_N^2\mathcal{M}^2}{\sqrt{1+\alpha}}\left(\frac{2}{r^3}\right)\left[1-\left(\frac{\alpha}{1+\alpha}\right)\frac{G_N\mathcal{M}}{2r}\right]\times\left(1+\frac{G_N^2\mathcal{M}^2}{1+\alpha}\frac{1}{r^2}\right)^{-\frac{3}{2}}\left(1-\frac{G_N\mathcal{M}}{r}\right)^{-1} \tag{31}$$

Case II: Along the equatorial plane ($\theta = \frac{\pi}{2}$), the LT precession frequency is

$$\Omega_{LT}=\frac{G_N^2\mathcal{M}^2}{\sqrt{1+\alpha}}\left(\frac{1}{r^3}\right)\left[1-\left(\frac{\alpha}{1+\alpha}\right)\frac{G_N\mathcal{M}}{r}\right]\times\left(1-2\frac{G_N\mathcal{M}}{r}+\frac{\left(\frac{\alpha}{1+\alpha}\right)G_N^2\mathcal{M}^2}{r^2}\right)^{-1} \tag{32}$$

and along the pole

$$\Omega_{LT}=\frac{2G_N\mathcal{M}\left[r-\left(\frac{\alpha}{1+\alpha}\right)\frac{G_N\mathcal{M}}{2}\right]}{a^3\sqrt{1+\left(\frac{\alpha}{1+\alpha}\right)\frac{G_N^2\mathcal{M}^2}{a^2}}} \tag{34}$$

This immediately implies that

$$\Omega_{LT}\propto\frac{1}{a^3} \tag{35}$$

and

$$\Omega_{LT}\propto\left[r-\left(\frac{\alpha}{1+\alpha}\right)\frac{G_N\mathcal{M}}{2}\right]\left[1+\left(\frac{\alpha}{1+\alpha}\right)\frac{G_N^2\mathcal{M}^2}{a^2}\right]^{-\frac{1}{2}} \tag{36}$$

For $\theta\neq\frac{\pi}{2}$ and in the superspinar limit, we find the exact LT frequency

$$\Omega_{LT}=\frac{G_N\mathcal{M}\left[r-\left(\frac{\alpha}{1+\alpha}\right)\frac{G_N\mathcal{M}}{2}\right]}{a^3\cos^4\theta}\left[1+\left(\frac{\alpha}{1+\alpha}\right)\frac{G_N^2\mathcal{M}^2}{a^2\cos^2\theta}\right]^{-1}\times\sqrt{4\left\{1+\left(\frac{\alpha}{1+\alpha}\right)\frac{G_N^2\mathcal{M}^2}{a^2}\right\}+\left(\frac{\tan\theta}{a}\right)^2\left(\frac{\alpha}{1+\alpha}\right)^2G_N^2\mathcal{M}^2\frac{\left\{r+\left(\frac{1+\alpha}{\alpha}\right)\frac{a^2\cos^2\theta}{G_N\mathcal{M}}\right\}^2}{\left(r-\left(\frac{\alpha}{1+\alpha}\right)\frac{G_N\mathcal{M}}{2}\right)^2}} \tag{37}$$

In each case we observe that the LT precession frequency is directly proportional to the $\frac{\mathcal{M}^2}{\sqrt{1+\alpha}}$, and is inversely proportional to the cubic value of radial distance parameter.

that means

$$\Omega_{LT} \propto \left[r - \left(\frac{\alpha}{1+\alpha}\right)\frac{G_N\mathcal{M}}{2}\right]\left[1 + \left(\frac{\alpha}{1+\alpha}\right)\frac{G_N^2\mathcal{M}^2}{a^2\cos^2\theta}\right]^{-1} \times \sqrt{4\left\{1 + \left(\frac{\alpha}{1+\alpha}\right)\frac{G_N^2\mathcal{M}^2}{a^2}\right\} + \left(\frac{\tan\theta}{a}\right)^2\left(\frac{\alpha}{1+\alpha}\right)^2 G_N^2\mathcal{M}^2\frac{\left\{r + \left(\frac{1+\alpha}{\alpha}\right)\frac{a^2\cos^2\theta}{G_N\mathcal{M}}\right\}^2}{\left(r - \left(\frac{\alpha}{1+\alpha}\right)\frac{G_N\mathcal{M}}{2}\right)^2}} \tag{38}$$

and

$$\Omega_{LT} \propto \frac{1}{a^3\cos^4\theta} \tag{39}$$

These are the fundamental differences between the NXBH, XBH and NS via computation of LT frequency. Also this is the main result of our work. Now we have to see their structural differences based on the graphical plot (Fig. 4).

## 3 Discussion

We studied the geometrical differences between NXBH and superspinar of Kerr BH in MOG theory in terms of precession of the spin of a test gyroscope due to the frame-dragging effect by the central rotating body. We found that there is indeed an crucial difference between these compact objects in the behavior of gyro spin precession frequency. For NXBH, we have found that the LT precession frequency varies as $\Omega_{LT} \propto a$ and $\Omega_{LT} \propto \frac{1}{r^3}$. While for XBH, the LT precession frequency varies as $\Omega_{LT} \propto \frac{\mathcal{M}^2}{\sqrt{1+\alpha}}$ and $\Omega_{LT} \propto \frac{1}{r^3}$. Note that the behavior of LT gyro precession of NXBH is qualitatively same as XBH. For NS, it varies as $\Omega_{LT} \propto \frac{1}{a^3}$ and $\Omega_{LT} \propto \left[r - \left(\frac{\alpha}{1+\alpha}\right)\frac{G_N\mathcal{M}}{2}\right]\left[1 + \left(\frac{\alpha}{1+\alpha}\right)\frac{G_N^2\mathcal{M}^2}{a^2}\right]^{-\frac{1}{2}}$ in the regime $\theta = 0$ and $a >> r$ limit. For $\theta \neq \frac{\pi}{2}$, we have found Eq. (38) and $\Omega_{LT} \propto \frac{1}{a^3\cos^4\theta}$. Using these specific criterion one can differentiate these compact objects. In summary, for a compact object like BH, the LT frequency varies as $\Omega_{LT} \propto a$ and $\Omega_{LT} \propto \frac{1}{r^3}$. While for superspinar, the LT frequency varies as $\Omega_{LT} \propto \frac{1}{a^3}$ and $\Omega_{LT} \propto \left[r - \left(\frac{\alpha}{1+\alpha}\right)\frac{G_N\mathcal{M}}{2}\right]\left[1 + \left(\frac{\alpha}{1+\alpha}\right)\frac{G_N^2\mathcal{M}^2}{a^2}\right]^{-\frac{1}{2}}$ along the pole. In the $\theta \neq \frac{\pi}{2}$ limit, the spin frequency is governed by Eq. (38) and also $\Omega_{LT} \propto \frac{1}{a^3\cos^4\theta}$. It is unlikely that Kerr BH in Einstein's general relativity where the precession frequency varies as only radial distance parameter.

**Data Availability Statement** This manuscript has no associated data. [Authors' comment: Data sharing not applicable to this article as no data sets were generated or analyzed during the current study.]

**Code Availability Statement** This manuscript has no associated code/software. [Authors' comment: Code/Software sharing not applicable to this article as no code/software was generated or analysed during the current study.]


Funded by SCOAP[3].

## References

1. J. Lense, H. Thirring, On the effect of rotating distant masses in Einstein's theory of gravitation. Physikalische Zeitschrift **19**, 156–163 (1918)
2. C.W. Misner, K.S. Thorne, J.A. Wheeler, *Gravitation* (W. H. Freeman & Company, New York, 1973)
3. L.I. Schiff, Possible new experimental test of general relativity theory. Phys. Rev. Lett. **4**, 215 (1960)
4. C.W.F. Everitt, D.B. De Bra, B.W. Parkinson, J.P. Turneaure, J.W. Conklin, M.I. Heifetz et al., Gravity probe B: final results of a space experiment to test general relativity. Phys. Rev. Lett. **106**, 221101 (2011)
5. P. Pradhan, Distinguishing black hole and naked singularity in MOG via inertial frame dragging effect. arXiv:2007.01347
6. C. Chakraborty, P. Kocherlakota, P.S. Joshi, Spin precession in a black hole and naked singularity spacetime. Phys. Rev. D **95**, 044006 (2017)
7. C. Chakraborty, P. Kocherlakota, M. Patil, S. Bhattacharyya, P.S. Joshi, A. Królak, Distinguishing Kerr naked singularities and black holes using the spin precession of a test gyro in strong gravitational fields. Phys. Rev. D **95**, 084024 (2017)
8. C. Chakraborty, S. Bhattacharyya, Circular orbits in Kerr–Taub-NUT spacetime and their implications for accreting black holes and naked singularities. JCAP **05**, 034 (2019)

9. J.W. Moffat, Black holes in modified gravity. Eur. Phys. J. C **75**, 175 (2015)
10. J.W. Moffat, Scalar-tensor-vector gravity theory. JCAP **0603**, 004 (2006)
11. J.W. Moffat, Modified gravity black holes and their observable shadows. Eur. Phys. J. C **75**, 130 (2015)
12. L. Manfredi, J. Mureika, J. Moffat, Quasinormal modes of modified gravity (MOG) black holes. Phys. Lett. B **779**, 492 (2018)
13. M.F. Wondrak, P. Nicolinia, J.W. Moffat, Superradiance in modified gravity. JCAP **12**, 021 (2018)
14. C. Chakraborty, P. Majumdar, Strong gravity Lense–Thirring precession in Kerr and Kerr–Taub-NUT spacetimes. Class. Quantum Gravity **31**, 075006 (2014)
15. C. Chakraborty, P. Pradhan, Lense–Thirring precession in Plebański–Demiański spacetimes. Eur. Phys. J. C **73**, 2536 (2013)
16. C. Chakraborty, P. Pradhan, Behavior of a test gyroscope moving towards a rotating traversable wormhole. JCAP **003**, 035 (2017)
17. C. Chakraborty, K.P. Modak, D. Bandyopadhyay, Dragging of inertial frames inside the rotating neutron stars. Astrophys. J. **790**, 2 (2014)
18. C. Chakraborty, O. Ganguly, P. Majumdar, Inertial frame dragging in an acoustic analogue spacetime. Ann. Phys. (Berlin) **530**, 1700231 (2017)
19. T. Jacobson, T.P. Sotiriou, Overspinning a black hole with a test body. Phys. Rev. Lett. **103**, 141101 (2009)
20. E. Barausse, V. Cardoso, G. Khanna, Test bodies and naked singularities: is the self-force the cosmic censor? Phys. Rev. Lett. **105**, 261102 (2010)
21. M. Colleoni, L. Barack, Overspinning a Kerr black hole: the effect of the self-force. Phys. Rev. D **91**, 104024 (2015)
22. K. Nakao, M. Kimura, T. Harada, M. Patil, P.S. Joshi, How small can an over-spinning body be in general relativity? Phys. Rev. D **90**, 124079 (2014)
23. A. Saa, R. Santarelli, Destroying a near-extremal Kerr–Newman black hole. Phys. Rev. D **84**, 027501 (2011)
24. Z. Li, C. Bambi, Super-spinning compact objects generated by thick accretion disks. JCAP **03**, 031 (2013)
25. F. de Felice, Classical instability of a naked singularity. Nature **273**, 8 (1978)
26. M. Calvini, F. de Felice, L. Nobili, Are naked singularities really visible? Lett. Nuovo Cimento **23**, 15 (1978)
27. H. Zhang, Naked singularity, firewall, and Hawking radiation. Sci. Rep. **7**, 4000 (2017)
28. P. Sheoren, A.H. Aguilar, U. Nucamendi, Mass and spin of a Kerr black hole in modified gravity and a test of the Kerr black hole hypothesis. Phys. Rev. D **97**, 124049 (2018)
29. K. Nakao et al., On the stability of a superspinar. Phys. Lett. B **780**, 410 (2018). (**and references therein**)